Chapter 9

Optical Properties of Antiferromagnetic/Ion-Crystalic Photonic Crystals

Shu-Fang Fu and Xuan-Zhang Wang

Additional information is available at the end of the chapter

http://dx.doi.org/10.5772/56397

1. Introduction

Increasing attention has been paid to magnetic photonic crystals (MPCs) because the properties of the MPCs can be modulated not only with the change of their structure (including components, layer thickness or thickness ratio) but also with the external magnetic field. MPCs are capable of acting as tunable filters [1] at different frequencies, and that controllable gigantic Faraday rotation angles [2-6] are simultaneously obtained. The nonmagnetic media in MPCs generally are ordinary dielectrics, so the electromagnetic wave modes are just magnetic polaritons. The effect of magnetic permeability and dielectric permittivity of two component materials in MPCs on the photonic band groups were discussed, where the permeability and permittivity were considered as scalar quantities [7].

Recently, our group investigated the optical properties of antiferromagnetic/ ion-crystal (AF/IC) PCs [8-11]. It is well known that the two resonant frequencies of AFs, such as, FeF2 and MnF2, fall into the millimeter or far infrared frequencies regions and some ionic semiconductors possess a very low phonon-resonant frequency range like the AFs. Especially, these frequency regions also are situated the working frequency range of THz technology, so the AF/IC PCs may be available to make the new elements in the field of THz technology. Note that in ICs, including ionic semiconductors, when the frequencies of the phonon and the transverse optical (TO) phonon modes of ICs are close, the dispersion curves of phonon and TO phonon modes will be changed and a kind of coupled mode called phonon polariton will be formed. Therefore, in the AF/IC PCs, the TO phonon modes of ICs can directly couple with the electric field in an electromagnetic wave and this coupling generates the phonon polaritons, however, the magnetization's motion in magnets can directly couple with the magnetic field, which is the origin of magnetic polaritons. Thus in such an AF/IC PCs, we refer to collective polaritons as the magneto-phonon polaritons (MPPs). In the presence of external magnetic field and damping, MPPs spectra display two

petty bulk mode bands with negative group velocity. It is worthy of mentioning that many surface modes emerge in the vicinity of two petty bulk mode bands, and that some surface modes bear nonreciprocality [11]. The optical properties of the AF/IC PCs can be modulated by an external magnetic field.

In addition, we have concluded that there is a material match of an AF and an IC, for which a common frequency range is found, in which the AF has a negative magnetic permeability and the IC has negative dielectric permittivity [10]. Consequently, the AF/IC structures are thought to be of the left-handed materials (LHMs) which have attracted much attention from the research community in recent years because of their completely different properties from right-handed materials (RHMs). In a LHM, the electric field, magnetic field and wave vector of a plane electromagnetic wave form a left-handed triplet, the energy flow of the plane wave is opposite in direction to that of the wave vector [12-17]. LHMs have to be constructed artificially since there is no natural LHM. Several variations of the design have been studied through experiments [18-20]. Up to now, scientists have found some LHMs available in infrared and visible ranges [21-25], but each design has a rather complicated structure. We noticed a work that discussed the left-handed properties of a superlattice composed of alternately semiconductor and antiferromagnetic (AF) layers, where the interaction between AF polaritons and semiconductor plasmons lead to the left-handedness of the superlattice [26]. However the plasmon resonant frequency sensitively depends on the free charge carrier's density, or impurity concentration in semiconductor layers, so if one wants to see a plasmon resonant frequency near to AF resonant frequencies, the density must be very low since AF resonant frequencies are distributed in the millimeter to far infrared range. In the case of such a low density, the effect of the charge carriers on the electromagnetic properties may be very weak [27] so that there is not the left-handedness of the superlattice. According the discussion above, we propose a simple structure of multilayer which consists of AF and IC layers. An analytical condition under which both left-handeness and negative refraction phenomenon appear in the film is established by calculating the angle between the energy flow and wave vector of a plane electromagnetic wave in AF/IC PCs and its refraction angle.

2. Magneto-phonon polaritons (MPPs) in AF/IC PCs

Polaritons in solids are a kind of electromagnetic modes determining optical or electromagnetic properties of the solids. Natures of various polaritons, including the surface and bulk polaritons, were very clearly discussed in Ref. [28]. Recent years, based on magnetic multilayers or superlattices, where nonmagnetic layers are of ordinary dielectric and their dielectric function is a constant, the polaritons in these structures called the MPCs were discussed [29-34]. On the other hand, ones were interested in the phonon polaritons [35-36], where the surface polariton modes could be focused by a simple way and probably possess new applications. In this part, the collective polaritons, MPPs in a superlattice structure comprised of alternating AF and IC layers, will be discussed. In the past, for simplicity, the damping was generally ignored in the discussion of dispersion properties

regarding the polaritons[30,32-34]. Actually, most materials are dispersive and absorbing. Therefore, it is also necessary to consider the effect of damping.

2.1. MPPs in one-dimension AF/IC PCs

An interesting configuration in experiment is the Voigt geometry as illustrated in Fig.1, where the polariton wave propagates in the *x-y* plane and the magnetic field of an electromagnetic wave is parallel to this plane, but the wave electric field aligns the *z* direction. We concentrate our attention on the case where the external magnetic field and AF anisotropy axis both are along the z axis and parallel to layers. The y axis is perpendicular to layers in the structure. The semi-space ($y<0$) is of vacuum, where d_a and d_i are thicknesses of AF and IC layers, respectively. For the far infrared wave, the order of the wavelength is about $100\mu m$. Thus, as long as the thicknesses of AF and IC layers are less than $10\mu m$, the wavelength λ will much longer than the period of AF/IC PCs. With this condition, the AF/IC PCs will become a uniform film by means of an effective-medium method (EMM).

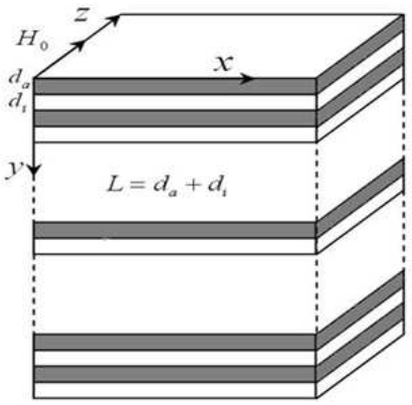

Figure 1. Illustration and coordinate system.

2.1.1. EMM for one-dimensional AF/IC PCs

We first present the permeability of the AF film. In the external magnetic field $\vec{H}_0$, the magnetic permeability is well-known, with its nonzero elements [33, 37]

$$\mu_{xx}=\mu_{yy}=\mu=1+\omega_m\omega_a\{[\omega_r^2-(\omega_0-\omega-\mathrm{i}\tau)^2]^{-1}+[\omega_r^2-(\omega_0+\omega+\mathrm{i}\tau)^2]^{-1}\}, \quad (1)$$

$$\mu_{xy}=-\mu_{yx}=\mu_{\perp}=i\omega_m\omega_a\{[\omega_r^2-(\omega_0-\omega-\mathrm{i}\tau)^2]^{-1}-[\omega_r^2-(\omega_0+\omega+\mathrm{i}\tau)^2]^{-1}\}. \quad (2)$$

with $\omega_0=\gamma H_0$, $\omega_m=4\pi\gamma M_0$, $\omega_a=\gamma H_a$, $\omega_e=\gamma H_e$, and $\omega_r=[\omega_a(2\omega_e+\omega_a)]^{1/2}$, where M_0 is the sublattice magnetization, H_a represents the anisotropy field, and H_e the exchange field. ω_r is the AF resonant frequency, γ the gyromagnetic ratio, and τ the magnetic damping constant. We use ε_a as the dielectric constant of the AF. Subsequently, we present the dielectric function of the IC [38],

$$\varepsilon_{\mathrm{i}} = \varepsilon_h + \frac{(\varepsilon_l - \varepsilon_h)\omega_T^2}{\omega_T^2 - \omega^2 - i\eta\omega}, \tag{3}$$

Where ε_h and ε_l are the high- and low-frequency dielectric constants, but ω_T is the TO resonant frequency of $k=0$ and η is the phonon damping coefficient. The IC is nonmagnetic, so its magnetic permeability is taken as $\mu_i = 1$.

We assume that there are an effective relation $\vec{B} = \vec{\mu}_{eff} \cdot \vec{H}$ between effective magnetic induction and magnetic field, and an effective relation $\vec{D} = \vec{\varepsilon}_{eff} \cdot \vec{E}$ between effective electric field and displacement, where these fields are considered as the wave fields in the structures. But $\vec{b} = \vec{\mu} \cdot \vec{h}$ and $\vec{d} = \varepsilon\vec{e}$ in any layer, where $\vec{\mu}$ is given in Eqs.(1) for AF layer and $\vec{\mu} = 1$ for IC layers. These fields are local fields in the layers. For the components of magnetic induction and field continuous at the interface, one assumes

$$H_x = h_{1x} = h_{2x}, H_z = h_{1z} = h_{2z}, B_y = b_{1y} = b_{2y}, \tag{4}$$

And for those components discontinuous at the interface, one assumes

$$B_x = f_a b_{1x} + f_i b_{2x}, B_z = f_a b_{1z} + f_i b_{2z}, H_y = f_a h_{1y} + f_i h_{2y}. \tag{5}$$

where the AF volume fraction $f_a = d_a / L$ and the IC volume fraction $f_i = d_i / L$ with the period $L = d_a + d_i$ .Thus the effective magnetic permeability is achieved from Eqs. (4),(5) and it is definite by $\vec{B} = \vec{\mu}_{eff} \cdot \vec{H}$,

$$\vec{\mu}_{eff} = \begin{pmatrix} \mu_{xx}^e & i\mu_{xy}^e & 0 \\ -i\mu_{xy}^e & \mu_{yy}^e & 0 \\ 0 & 0 & 1 \end{pmatrix}, \tag{6}$$

with the elements

$$\mu_{xx}^{\mathrm{e}} = \mathrm{f_a}\mu + \mathrm{f_i} - (\mathrm{f_a f_i}\mu_{\perp}^2)/(\mu \mathrm{f_i} + \mathrm{f_a}),\ \mu_{yy}^{\mathrm{e}} = \mu/(\mu \mathrm{f_i} + \mathrm{f_a}),\ \mu_{xy}^{\mathrm{e}} = \mu_{yx}^{\mathrm{e}} = \mathrm{f_a}\mu_{\perp}/(\mu \mathrm{f_i} + \mathrm{f_a}), \tag{7}$$

On the similar principle, we can find that the effective dielectric permittivity tensor is diagonal and its elements are

$$\varepsilon_{xx}^e = \varepsilon_{zz}^e = f_a\varepsilon_a + f_i\varepsilon_i,\ \varepsilon_{yy}^e = \varepsilon_a\varepsilon_i / (f_a\varepsilon_a + f_i\varepsilon_i). \tag{8}$$

On the base of these effective permeability and permittivity, one can consider the AF/IC PCs as homogeneous and anisotropical AF films or bulk media. The similar discussions can be found in the Chapter 3 of the book "Propagation of Electromagnetic Waves in Complex Matter" edited by Ahmed Kishk [39].

2.1.2. Dispersion relations of surface and bulk MPP with transfer matrix method (TMM)

The wave electric fields in an AF layer and IC layer are written as

$$\vec{\mathrm{E}} = (E_A e^{\alpha y} + E_B e^{-\alpha y}) \exp(ikx - i\omega t)\vec{\mathrm{e}}_z, \tag{9}$$

$$\vec{\mathrm{E}} = (E_C e^{\beta y} + E_D e^{-\beta y}) \exp(ikx - i\omega t)\vec{\mathrm{e}}_z, \tag{10}$$

respectively. k is the wave-vector component along x axis. α and β are the decay coefficients when they are real, otherwise they correspond to the y wave-vector components. E_j (j=*A, B, C or D*) denotes the amplitudes of the electric fields. Additionally, the corresponding magneticfields can be found with the relation $\nabla \times \vec{E} = i\omega\vec{B}$. The wave equation resulting from the Maxwell equations is

$$\nabla(\nabla \cdot \vec{E}) - \nabla^2 \vec{E} - \mu_0 \omega^2 / c^2 \, \vec{\varepsilon} \cdot \vec{E} = 0. \tag{11}$$

We see from the wave equation that

$$\alpha^2 = k^2 - \varepsilon_a \mu_v \omega^2 / c^2 \tag{12}$$

with $\mu_{\mathrm{v}} = (\mu^2 - \mu_\perp^2)/\mu$ and c is the light velocity in vacuum, and

$$\beta^2 = k^2 - \varepsilon_i \omega^2 / c^2 . \tag{13}$$

Employing the well-known TMM, together withthe boundary conditions of E_z and H_x continuous at the interfaces, we can find a matrix relation between wave amplitudes in any two adjacent bi-layers, or the relation between amplitudes in the nth and n+1th bi-layers

$$\begin{pmatrix} E_{an+1} \\ E_{bn+1} \end{pmatrix} = T \begin{pmatrix} E_{an} \\ E_{bn} \end{pmatrix} \tag{14}$$

where T is the transfer matrix expected and its components are

$$T_{11} = \frac{e^{\alpha d_a}}{\Delta - \Delta'}[(\Delta - \Delta')\cosh(\beta d_i) + (1 - \Delta\Delta')\sinh(\beta d_i)],\ T_{12} = \frac{e^{-\alpha d_a}(1 - \Delta'^2)}{\Delta - \Delta'}\sinh(\beta d_i), \tag{15}$$

$$T_{21} = \frac{e^{\alpha d_a}(\Delta^2 - 1)}{\Delta - \Delta'}\sinh(\beta d_i),\ T_{22} = \frac{e^{-\alpha d_a}}{\Delta - \Delta'}[(\Delta - \Delta')\cosh(\beta d_i) + (\Delta\Delta' - 1)\sinh(\beta d_i)], \tag{16}$$

with $\Delta = (\alpha\mu - k\mu_\perp)/[\beta(\mu^2 - \mu_\perp^2)]$ and $\Delta' = -(\alpha\mu + k\mu_\perp)/[\beta(\mu^2 - \mu_\perp^2)]$. The Bloch's theorem implies another relation

$$\begin{pmatrix} E_{an+1} \\ E_{bn+1} \end{pmatrix} = e^{iQL} \begin{pmatrix} E_{an} \\ E_{bn} \end{pmatrix}. \tag{17}$$

Based on matrix relations (14) and (17), we obtain the polariton dispersion equation

$$\cos(QL) = \cosh(\alpha d_a)\cosh(\beta d_i) + (\frac{\beta\mu_v}{2\alpha} + \frac{k^2 - \varepsilon_a \mu \omega^2 / c^2}{2\alpha\beta\mu})\sinh(\alpha d_a)\sinh(\beta d_i). \quad (18)$$

Q is the Bloch wave number for an infinite structure and is a real number, and then equation (18) describes the bulk polariton modes.

For a semi-infinite structure, it is interesting in physics that $Q = i\rho$ is an imaginary number. Thus equation (18) can be used to determine the surface modes traveling along the x axis. We need the electromagnetic boundary conditions at the surface of this structure to find another necessary equation for the surface polariton modes. This equation is just

$$T_{11} + \varphi T_{12} = \exp(-\rho L) = \varphi^{-1} T_{21} + T_{22}, \quad (19)$$

where $\varphi = (\Delta\beta - \alpha_0)/(\alpha_0 - \Delta'\beta)$ with $\alpha_0^2 = k^2 - \omega^2/c^2$. α_0 is the decay coefficient in vacuum and must be positive. It needs to be emphasized that the existence of surface modes requires Re(ρ) >0 .Eqs. (18) and (19) will be applied to determine the bulk polariton bands and surface polaritons.

Numerical simulations based on FeF_2/TlBr will be performed with TMM. The reason is that their resonant frequencies lie in the far infrared range and are close to each other. The physical parameters here applied are $H_e = 533\text{kG}$, $4\pi M_0 = 7.04\text{kG}$, $H_a = 197\text{kG}$, $\varepsilon_a = 5.5$, $\eta = 5\times10^{-4}$, and $\omega_r = 498.8\text{kG}$ ($\approx 52.45 cm^{-1}$) for AF layers; $\varepsilon_l = 30.4$, $\varepsilon_h = 5.34$, $\omega_T = 48 cm^{-1}$, $\xi = 8\times10^{-3}$ for IC layers. The external field $H_0 = 3.0T$ [10,33,34].

The MPP spectra are displayed in Fig.2, 3, and 5. In these spectra for dimensionless reduced f

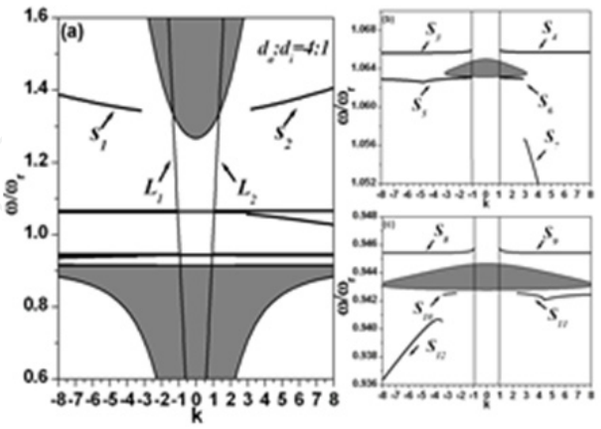

Figure 2. Bulk polariton bands (shaded areas) and surface polaritons (thick solid curves) for $d_a / d_i = 4:1$ via TMM: (a) a whole dispersion pattern; (b) and (c) are the partially enlarged figures. After Wang & Ta, 2010.

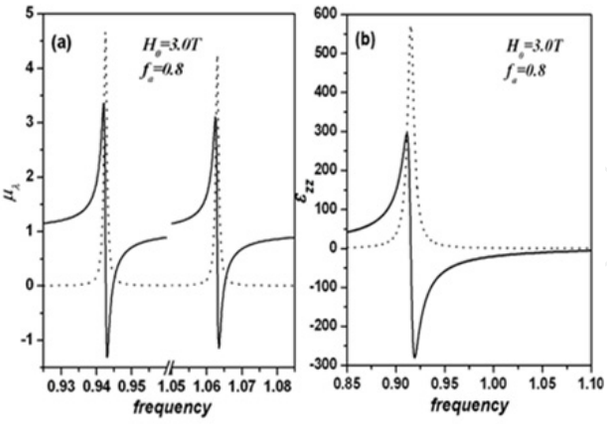

Figure 3. Effective magnetic permeability and dielectric function for $d_a / d_i = 4:1$. (a) The magnetic permeability and (b) the dielectric function. After Wang & Ta, 2010.

The MPP spectra are displayed in Fig.2, 3, and 5. In these spectra for dimensionless reduced frequency ω/ω_r versus k, the shaded regions stand for the bulk bands whose boundaries are determined by Eq. (18) or (19) with $Q = 0$ and $k = 0$, respectively. Meanwhile, the surface modes are obtained by Eqs. (18), (19) and (21). The thick curves with the serially numbered sign S denote the surface polaritons. The photonic lines $k^2 = (\omega / c)^2$ in vacuum are labeled as L_1 and L_2.Fig.2 shows the bulk bands and surface modes for the ratio $d_a / d_i = 4:1$ $(f_a = 0.8)$, which are obtained by the TMM. Four bulk continua appear including two minibands (see Figs. 2(b) and 2(c)). The top and bottom bands (see Fig.2(a)) correspond to the positive real parts of the effective magnetic permeability and dielectric function, so the effective refraction index is positive in the two bands. However, the two mini bands (see Figs.2(b) and 2(c)) are related to the negative real parts of the permeability and dielectric function, which can be found from Fig.3. It means that the effective refraction index is negative in the mini bands. Ref.14 proved that the negative refraction and left-handedness exist in the mini bands, where the transmission and refraction of the same structure were examined in the absence of the external magnetic field.

Fig.4 displays the bulk bands and surface modes for ratio $d_a / d_i = 1:1$. The top bulk band is distinctly ascended to the high frequency direction, together with surface mode 1and 2. The bottom bulk band is widened conspicuously. Contrary to the previous situation, the two mini bands get significantly narrower. Compared with Fig.2, the slopes of surface modes 7 and 12 diminish appreciably, meaning their group velocity dwindles as the AF volume fraction (f_a) decreases.

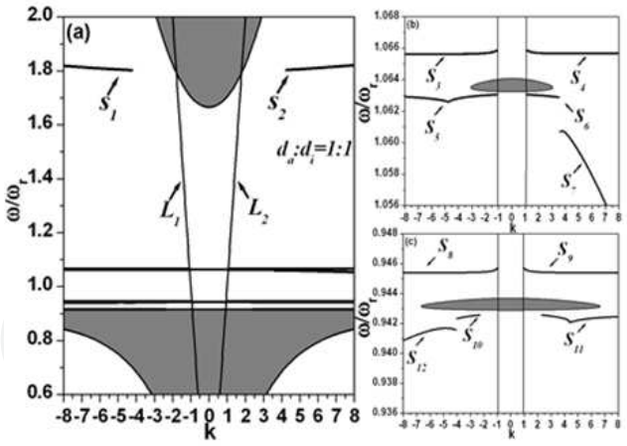

Figure 4. Bulk polariton bands and surface modes with the parameters and explanations as the same as those in Fig.2, except for $d_a / d_i = 1:1$. After Wang & Ta, 2010.

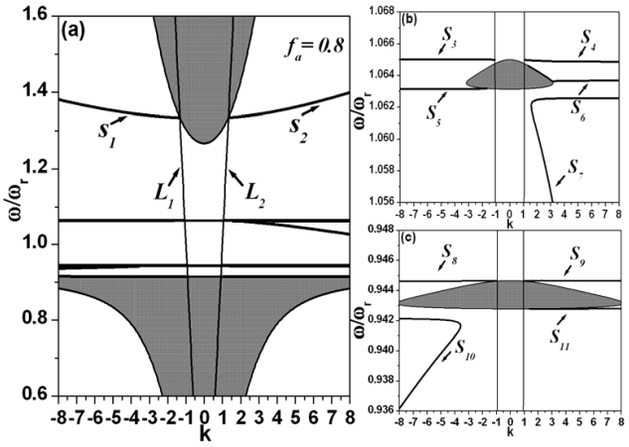

Figure 5. Bulk polariton bands and surface polaritons for $d_a / d_i = 4:1$. The interpretations of (a), (b) and (c) are the same as those of Fig.2. After Wang & Ta, 2010.

2.1.3. Limiting case of small period (EMM)

To examine the limiting case of small period or long wavelength is meaningful in physics. We let $d_a \to 0$ and $d_i \to 0$ in Eqs.(18) ,(19) and then find

$$Q^2 + (\mu_{xx}^e / \mu_{yy}^e)k^2 - \varepsilon_{zz}^e \mu_\lambda^e (\omega / c)^2 = 0, \tag{20}$$

for the bulk modes with $\mu_\lambda^e = (\mu_{xx}^e \mu_{yy}^e - \mu_{xy}^{e2}) / \mu_{yy}^e$, and

$$\rho + (\mu_{xy}^e / \mu_{yy}^e)k + \alpha_0 \mu_\lambda^e = 0,\ \rho^2 = (\mu_{xx}^e / \mu_{yy}^e)k^2 - \varepsilon_{zz}^e \mu_\lambda^e (\omega / c)^2 = 0, \tag{21}$$

for the surface polaritons. If the external magnetic field implicitly included in Eqs.(20) and (21) is equal to zero, the dispersion relations can be reduced to those in our earlier paper [10].Hence equations (20) and (21) also can be considered as the results achieved by the EMM.

Fig.5 shows the bulk bands and surface modes for the ratio $d_a / d_i = 4:1$ ($f_a = 0.8$), which are obtained by the EMM. For the bulk bands, we see that the results obtained within the two methods almost are equal. However, the surface modes obtained by the EMM start from the photonic lines and are continuous, but those achieved by the TMM do not. It is because the interfacial effects are efficiently considered within the TMM, but the EMM neglects these. For the surface polaritons, their many main features attained by the two methods are still analogous. 12 surface mode branches are seen from Fig.2 within the TMM, but 11 surface modes from Fig.5 within the EMM. 10 surface mode branches arise in the common vicinities of two AF resonant frequencies and TO phonon frequency.Except branches 1 and 2, all surface modes are nonreciprocal and their non-reciprocity results from the magnetic contribution in AF layers. Surface polaritons 1 and 2 should be called the quasi-phonon polaritons since the contribution of the magnetic response to the polaritons is very weak in their frequency range. Another interesting feature is that many surface modes possess negative group velocities ($d\omega/dk < 0$), which is due to the combined contributions of magnetic damping and phonon damping.

2.2. MPPs in two-dimension AF/IC PCs

In this part, we consider such an AF/IC PCs constructed by periodically embedding cylinders of ionic crystal into an AF, as shown in Fig.6. We focus our attention on the situation where the external magnetic field and the AF anisotropy axis both are along the cylinder axis, or the *z*-axis. The surface of the MPC is parallel to the *x*-*z* plane. L and R indicate the lattice constant and cylindrical radius, respectively. We introduce the AF filling ratio, $f_a = 1 - \pi R^2 / L^2$, and the IC filling ratio, $f_i = \pi R^2 / L^2$. Our aim is to determine general characteristics of the surface and bulk polaritons with an effective-medium method under the condition of $\lambda >> L$ (λ is the polariton wavelength).

2.2.1. EMM for the two-dimensional AF/IC PCs

When the AF/IC PCs cell size is much shorter than the wavelength of electromagnetic wave, an EMM can be established for one to obtain the effective permeability and permittivity of the AF/IC PCs. The principle of this method is in a cell, an electromagnetic-field component continuous at the interface is assumed to be equal in the two media and equal to the corresponding effective-field component in the MPC, but one component discontinuous at the interface is averaged in the two media into another corresponding effective-field component [30,33,40-41]. Because the interface between the two media is of cylinder-style, before establishing an EMM, a TMM should be introduced. This matrix is

$$T = \begin{pmatrix} \cos\theta & \sin\theta & 0 \\ -\sin\theta & \cos\theta & 0 \\ 0 & 0 & 1 \end{pmatrix}, \tag{22}$$

Thus, we find the expression of the permeability in the cylinder coordinate system

$$\ddot{\mu}_a = T\ddot{\mu}_a' T^{-1} = \begin{pmatrix} \mu_{rr} & \mu_{r\theta} & 0 \\ -\mu_{r\theta} & \mu_{\theta\theta} & 0 \\ 0 & 0 & 1 \end{pmatrix}. \tag{23}$$

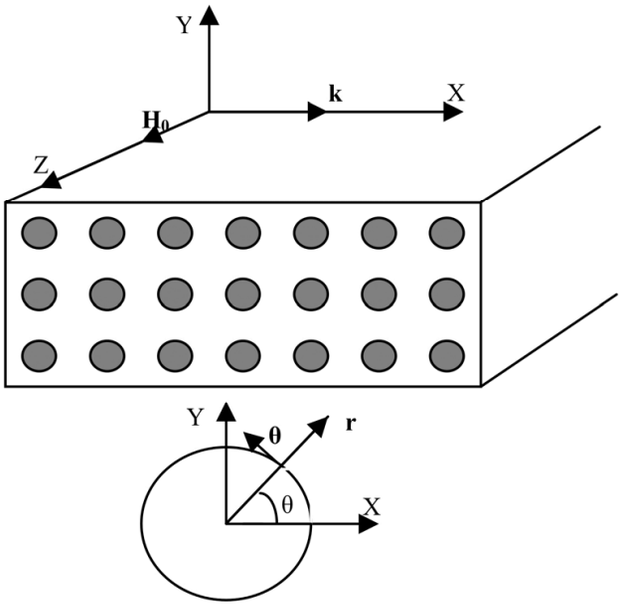

Figure 6. Geometry configuration and coordinate system.

with $\mu_{rr} = \mu_{\theta\theta} = \mu_{xx}$ and $\mu_{r\theta} = \mu_{xy}$. The theoretical processes of obtaining effective magnetic permeability, $\ddot{\mu}^e$, and electric permittivity, $\ddot{\varepsilon}^e$, are presented as follows. According to the principle,we can introduce the following equations:

$$H_z = h_{az} = h_{iz},\ H_\theta = h_{a\theta} = h_{i\theta}, \tag{24}$$

$$B_r = b_{ar} = b_{ir}, \tag{25}$$

$$H_r = f_a h_{ar} + f_i h_{ir}, \tag{26}$$

$$B_\theta = f_a b_{a\theta} + f_i b_{i\theta},\ B_z = f_a b_{az} + f_i b_{iz}, \tag{27}$$

where the field components on the left side of Eqs. (24)-(27) are defined as the effective components in the AF/IC PCs and those on the right side are the field components in the AF and IC media within the cell. In the AF, the relation between $\boldsymbol{b}$ and $\boldsymbol{h}$ is determined by (23) in the $r\theta z$ system, but in the IC, the relation is

$$\vec{b} = \vec{h}. \tag{28}$$

After defining the relation between the effective fields in the AF/IC PCs, $\vec{B} = \ddot{\mu}^e \cdot \vec{H}$, the effective permeabilityresulting from (24)-(27) is

$$\vec{\mu}^{e} = \begin{pmatrix} \mu^{e}_{rr} & \mu^{e}_{r\theta} & 0 \\ -\mu^{e}_{r\theta} & \mu^{e}_{\theta\theta} & 0 \\ 0 & 0 & 1 \end{pmatrix}, \tag{29}$$

with

$$\mu^{e}_{rr} = \mu_{rr} / (f_a + \mu_{rr} f_i) \tag{30}$$

$$\mu^{e}_{\theta\theta} = f_a \mu_{rr} + f_i + f_a f_i \mu^{2}_{r\theta} / (f_a + \mu_{rr} f_i) \tag{31}$$

$$\mu^{e}_{r\theta} = \mu_{r\theta} f_a / (f_a + \mu_{rr} f_i) = -\mu^{e}_{\theta r}. \tag{32}$$

Formula (29) is the expression of the effective magnetic permeability in the $r\theta z$ system. When we discuss the surface polaritons, the AF/IC PCs will be considered as a semi-infinite system with a single plane surface, so the corresponding permeability in the rectangular coordinate system (orthe xyz system) will be used. Applying the transformation matrix (22) again, we find

$$\vec{\mu}^{e}_{\perp} = \begin{pmatrix} \mu^{e}_{rr}\cos^2\theta + \mu^{e}_{\theta\theta}\sin^2\theta & (\mu^{e}_{rr} - \mu^{e}_{\theta\theta})\sin\theta\cos\theta + \mu^{e}_{r\theta} & 0 \\ (\mu^{e}_{rr} - \mu^{e}_{\theta\theta})\sin\theta\cos\theta - \mu^{e}_{r\theta} & \mu^{e}_{rr}\sin^2\theta + \mu^{e}_{\theta\theta}\cos^2\theta & 0 \\ 0 & 0 & 1 \end{pmatrix}. \tag{33}$$

If one applies directly this form into the Maxwell equations, the resulting wave equation will be very difficult to solve. Thus, a further approximation is necessary. We think that if the wavelength of an electromagnetic wave is much longer than the cell size, then the wave will feel very slightly the structure information of the AF/IC PCs. Here, the averages of some physics quantities are important. Hence, $\vec{\mu}^{e}_{\perp}$ is averaged with respect to angle θ and one determines the averaged effective magnetic permeability,

$$\vec{\mu}^{e}_{\perp a} = \begin{pmatrix} (\mu^{e}_{rr} + \mu^{e}_{\theta\theta})/2 & \mu^{e}_{r\theta} & 0 \\ -\mu^{e}_{r\theta} & (\mu^{e}_{rr} + \mu^{e}_{\theta\theta})/2 & 0 \\ 0 & 0 & 1 \end{pmatrix}. \tag{34}$$

This means $\mu^{e}_{xx} = \mu^{e}_{yy} = \mu^{e}$. In physics, this AF/IC PCs should be gyromagnetic and be of C4-symmetry, as shown by Fig.1, which leads to the *xx* and *yy* elements of the final permeability should be equal and its xy element equal to *-yx* element.

By a similarprocedure, the effective dielectric permittivity can be easily found. According to the principle of EMM, we present the equations for the electric-field and electric-displacement components as follows,

$$E_z = \mathrm{e}_{az} = e_{iz},\ E_\theta = \mathrm{e}_{a\theta} = e_{i\theta},\ D_r = d_{ar} = d_{ir}, \tag{35}$$

$$D_Z = f_a d_{az} + f_i d_{iz},\ D_\theta = f_a d_{a\theta} + f_i d_{i\theta},\ E_r = f_a \mathrm{e}_{ar} + f_i e_{ir}, \tag{36}$$

with $\vec{d}_{a(i)} = \varepsilon_{a(i)}\vec{e}$ in the AF or IC. After using the definition, $\vec{D} = \vec{\varepsilon}^{\,e}\vec{E}$, the effective dielectric permittivity of the AF/IC PCs in the $r\theta z$ system is determined as

$$\vec{\varepsilon}^{\,e} = \begin{pmatrix} \varepsilon^e_{rr} & 0 & 0 \\ 0 & \varepsilon^e_{\theta\theta} & 0 \\ 0 & 0 & \varepsilon^e_{zz} \end{pmatrix}, \tag{37}$$

With

$$\varepsilon^e_{rr} = \varepsilon_a\varepsilon_i \big/ (f_a\varepsilon_i + f_i\varepsilon_a),\ \varepsilon^e_{\theta\theta} = f_a\varepsilon_a + f_i\varepsilon_i,\ \varepsilon^e_{zz} = f_a\varepsilon_a + f_i\varepsilon_i \tag{38}$$

Transforming (37) into the form for the *xyz* system, we see

$$\vec{\varepsilon}^{\,e}_{\perp} = \begin{pmatrix} \varepsilon^e_{rr}\cos^2\theta + \varepsilon^e_{\theta\theta}\sin^2\theta & \varepsilon^e_{rr}\cos\theta\sin\theta - \varepsilon^e_{\theta\theta}\sin\theta\cos\theta & 0 \\ \varepsilon^e_{rr}\cos\theta\sin\theta - \varepsilon^e_{\theta\theta}\sin\theta\cos\theta & \varepsilon^e_{rr}\sin^2\theta + \varepsilon^e_{\theta\theta}\cos^2\theta & 0 \\ 0 & 0 & \varepsilon^e_{zz} \end{pmatrix}. \tag{39}$$

Then, its average value with respect to angle θ is

$$\vec{\varepsilon}^{\,e}_{\perp a} = \begin{pmatrix} (\varepsilon^e_{rr} + \varepsilon^e_{\theta\theta})/2 & 0 & 0 \\ 0 & (\varepsilon^e_{rr} + \varepsilon^e_{\theta\theta})/2 & 0 \\ 0 & 0 & \varepsilon^e_{zz} \end{pmatrix}. \tag{40}$$

We see $\varepsilon^e_{xx} = \varepsilon^e_{yy} = \varepsilon^e$. Now, this AF/IC PCs can be considered as an effective medium with effective electric permittivity $\vec{\varepsilon}^{\,e}_{\perp a}$ and magnetic permeability $\vec{\mu}^{\,e}_{\perp a}$. If the AF medium is taken as FeF_2 with its resonant frequency about $\omega_r / 2\pi c = 52.45 cm^{-1}$, proper wavelengths should be between 170 and 190μm. When the cell size is taken as μm order of magnitude, such as $5\mu m$, the effective-medium theory is available and expressions (34) and (40) are reasonable.

2.2.2. Dispersion equations of surface and bulk MPP

The effective permittivity (40) and permeability (34) are applied to determine the dispersion equations of surface and bulk MPP in the AF/IC PCs. In the geometry of Fig.6, if the magnetic field of a plane electromagnetic wave is along the *z*-axis, the sublattice magnetizations in the AF do not couple with it, so the AF plays a role of an ordinary dielectric. Thus, we propose the electric fields of polariton waves in the AF/IC PCs are along the *z*-axis and the magnetic field is in the *x*-*y* plane. For a surface polariton, its electric field decaying with distance from the surface can be written as

$$\vec{E} = [E_0 \exp(-\alpha_0 y)\exp(ikx - i\omega t)]\vec{e}_z, (y > 0) \tag{41}$$

$$\vec{E} = [E_1 \exp(\alpha y)\exp(ikx - i\omega t)]\vec{e}_z, (y < 0) \tag{42}$$

in the AF/IC PCs, where k is the wave-vector component along the x-axis, but α and α_0 are the decay coefficients and are positive for the surface polariton. The corresponding magneticfield can be obtained with the relation $\nabla \times \vec{E} = i\omega\vec{B}$. From the Maxwell equations, we confirm the electric field obeys the wave equations

$$\nabla^2\vec{E} + (\omega/c)^2\vec{E} = 0, (y > 0) \tag{43}$$

$$\nabla^2\vec{E} + (\omega/c)^2\varepsilon_{zz}^e\mu_v^e\vec{E} = 0, (y < 0) \tag{44}$$

which lead to two relations

$$\alpha_0^2 = \mathrm{k}^2 - (\omega/c)^2, \alpha^2 = \mathrm{k}^2 - \varepsilon_{zz}^{\mathrm{e}}\mu_{\mathrm{v}}^e(\omega/c)^2 \tag{45}$$

with $\mu_v^e = [(\mu^e)^2 + (\mu_{r\theta}^e)^2)]/\mu^e$. The dispersion relation can be found from the boundary conditions of the field components, E_z and H_x, continuous at the surface. Through a simple mathematical process, we obtain this relation

$$\alpha = -i\mu_{r\theta}^e \mathrm{k}/\mu^e - \alpha_0\mu_v^e, \tag{46}$$

where α and α_0 are determined by (45) with the conditions, $\alpha > 0$ and $\alpha_0 > 0$. Of course, it is very easy to find the dispersion relation of bulk polaritons. For the infinite AF/IC PCs, we find from the wave equation (44) that the dispersion relation in the x-y plane is

$$\mathrm{k}^2 = \varepsilon_{zz}^{\mathrm{e}}\mu_{\mathrm{v}}^e(\omega/c)^2 \tag{47}$$

The bulk polariton bands are just such regions determined by (46). One can calculate directly the dispersion curves of the surface polariton from (45).

FeF2 and TlBr are utilized as constituent materials in the AF/IC PCs, which the parameters have been introduced in the last section. We place the AF/IC PCs into an external field of $H_0 = 5.0T$ along the z-axis and employ a dimensionless reduced frequency $\omega/\omega_{\mathrm{r}}$ in figures. Surface mode curves are plotted against wave vector k along the x-axis. Bulk modes form some continuous regions shown with shaded areas.

For comparison, we first present the polariton dispersion figures in the AF FeF2 and IC TlBr, as indicated in Fig. 7, respectively. For the AF, there exist three bulk bands and two surface modes. The surface modes appear in a nonreciprocal way and have a positive group velocity ($d\omega/dk > 0$). For the IC, its surface modes and bulk bands are depicted in Fig. 7(b). The surface modes are of reciprocity. Comparing Fig. 7(b) with the previous results without phonon damping [42], it is different that the two surface modes bear bended-back and end on the vacuum light line, due to the phonon damping.

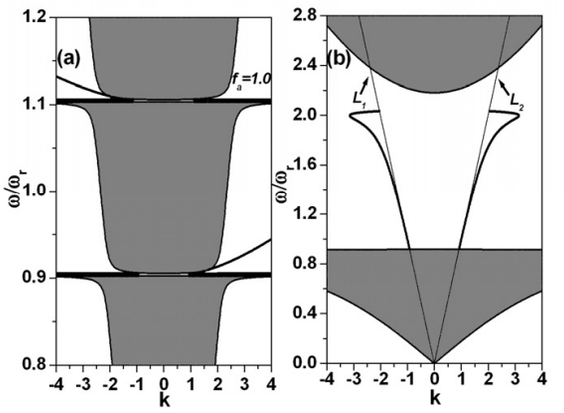

Figure 7. (a) Bulk polariton bands (shaded regions) and surface polaritons of FeF_2. (b) Bulk polariton bands and surface modes of TlBr, with two vacuum light lines (thin lines). After Wang & Ta, 2012.

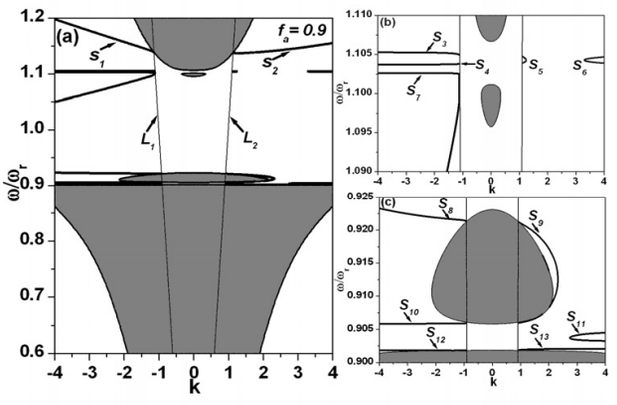

Figure 8. Bulk polariton bands (shaded regions) and surface polaritons of the MPC for $f_a = 0.9$: (a) a whole dispersion pattern;(b) and (c) are the partially amplified figures. After Wang & Ta, 2012.

For the AF/IC PCs with $f_a = 0.9$, Fig. 8 illustrates the dispersion features of magneto-phonon polaritons. Four bulk bands and 13 surface mode branches are found, where the surface modes are nonreciprocal (meaning the surface modes are changed when reversing their propagation directions). Two mini bulk bands and 11 surface mode branches exist in the vicinities of two AF resonant frequencies, where they are neither similar to those of the AF nor to those of the IC. Due to the combined contributions of the magnetic damping and phononic damping, the surface-mode group velocities become negative in some frequency ranges. For frequencies near the higher AF resonant frequency, the top bulk band bears a resemblance in nature to the top one of the AF, but the bottom band is analogous to the bottom one of the IC for frequencies close to the IC resonant frequency.

Figure 9 shows the bulk bands and surface modes for $f_a = 0.8$. The bulk bands in this figure are characteristically similar to those in Fig. 8, but the two mini bands are narrowed and the top one risesstrikingly. For the surface modes, mode 6 in Fig. 8 splits into two surface modes in Fig. 9. Modes 5 and 11 in Fig. 8 disappear from the field of view. The surface modes are still nonreciprocal.

The two mini bulk bands possess a special interest, corresponding to the negative effective magnetic permeability and negative effective dielectric permittivity of the AF/IC PCs. We present Fig. 10 for $f_a = 0.8$ to display the relevant effective permeability and permittivity. One can see that dielectric permittivity, ε_{zz}^{e}, is negative in a large frequency range. The two AF resonant frequencies lie in this range and the magnetic permeability, μ^{e}, is negative in the vicinities of the AF resonant frequencies. Thus, for electromagnetic waves traveling in the *x*-*y* plane, the refraction index is negative and the left-handedness can exist in the two mini bulk bands. When electromagnetic waves propagate along the *z*-axis, there is no coupling between AF magnetizations and electromagnetic fields, so the electromagnetic waves cannot enter this range where $\varepsilon^{e} < 0$ (see Eq. (1-30b)). The negative refraction and left-handedness were predicted in a one-dimension structure composed of identical materials [10].

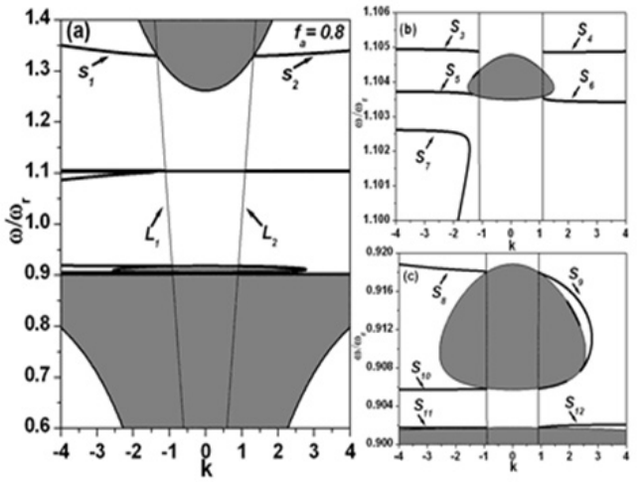

Figure 9. Bulk polariton bands and surface polaritons of the MPC for . The explanations of (a), (b) and (c) are identical to those of Fig.8. After Wang & Ta, 2012.

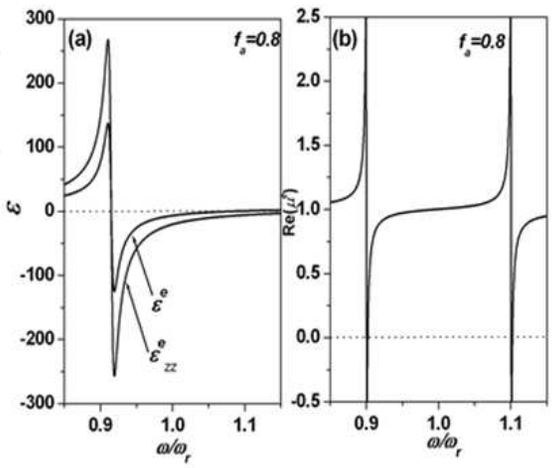

Figure 10. Effective permittivity and permeability in the MPC for : (a) the effective permittivity and (b) the effective permeability. After Wang & Ta, 2012.

3. Presence of left-handedness and negative refraction of AF/IC PCs

In the previous section, we have discussed MPPs in AF/IC PCs with the TMM and EMM for one- and two-dimension. Based on FeF_2/TIBr, there are a number of surface and bulk polaritons in which the negative refraction and left-handedness can appear. In order to investigate the formation mechanism of LHM in AF/IC PCs, the external magnetic field and magnetic damping is set to be zero. In this case, according Eqs.(7) and (8), the effective permeability $\ddot{\mu}^e$ and dielectric permittivity $\ddot{\varepsilon}^e$ will be described as

$$\mu_{xx}^e = (f_a\mu + f_i),\ \mu_{yy}^e = \mu/(f_a + f_i\mu),\ \mu_{zz}^e = 1, \tag{48}$$

$$\varepsilon_{xx}^e = \varepsilon_{yy}^e = \varepsilon_a\varepsilon_i/(f_a\varepsilon_i + f_i\varepsilon_a),\ \varepsilon_{zz}^e = (f_a\varepsilon_a + f_i\varepsilon_i), \tag{49}$$

where $f_a = d_a/D$ is the AF filling ratio, and $f_i = d_i/D$ is IC filling ratio with $D = d_i + d_a$ as a bi-layer thickness.

Let us consider an incident plane electromagnetic wave propagating in the x-y plane as shown in Fig.11. Such a wave can be divided into two polarizations, a TE mode with its electric field parallel to axis z and a TM mode with its magnetic field parallel to axis z. According to Maxwell's equations, these wave vectors and frequencies of the two modes inside the film satisfy the following expressions

$$\frac{k_y^2}{\varepsilon_{zz}^e\mu_{xx}^e} + \frac{k_x^2}{\varepsilon_{zz}^e\mu_{yy}^e} = (\omega/c)^2 \quad \left(for\ TE\ mode\right), \tag{50}$$

$$k_y^2 + k_x^2 = (\omega/c)^2\varepsilon_{xx}^e\mu_{zz}^e \ \left(for\ TE\ mode\right), \tag{51}$$

Since $\mu_{zz}^e = 1$ is a positive real number, relation (51) corresponds to the case of an ordinary optical (when $\varepsilon_{xx}^e > 0$) or an opaque (when $\varepsilon_{xx}^e < 0$, contributing to an imaginary k_y) film, and so, we no longer consider the TM case, but deal with only the case of TE incident mode, and found the left-handed feature and negative refraction behavior. For the TE mode, the presence of left-handed feature (or negative refraction) needs the satisfaction of the prerequisite condition that $\varepsilon_{zz}^e < 0$ and μ_{xx}^e and μ_{yy}^e can not be simultaneously positive [i.e., at least one of μ_{xx}^e and μ_{yy}^e is negative, see (50)]. According to expressions (48) and (49),

$$\omega_T \le \omega \le \omega_T\sqrt{1 + f_i(\varepsilon_0 - \varepsilon_\infty)/(f_a\varepsilon_a + f_i\varepsilon_\infty)}\ (for\ \varepsilon_{zz}^e < 0), \tag{52}$$

$$\omega_r \le \omega \le \sqrt{\omega_r^2 + 2f_a\omega_a\omega_m}\ (for\ \mu_{xx}^e < 0), \tag{53}$$

$$\sqrt{\omega_r^2 + 2f_i\omega_a\omega_m} \le \omega \le \sqrt{\omega_r^2 + 2\omega_a\omega_m}\ (for\ \mu_{yy}^e < 0), \tag{54}$$

where $\omega_a = \gamma H_a$ and $\omega_m = 4\pi\gamma M_0$. Frequency region (52) is very large and covers regions (53) and (54) for the selected physical parameters. It is noted that both $\mu_{xx}^e < 0$ and $\mu_{yy}^e < 0$

can occur simultaneously only when AF layers are thicker than IC layers, which corresponds to spectral domain $(\omega_r^2 + 2f_i\omega_a\omega_m)^{1/2} \le \omega \le (\omega_r^2 + 2f_a\omega_a\omega_m)^{1/2}$ .The wave electric field in the film can be written at

$$E_z = [A_0 \exp(ik_y y) + B_0 \exp(-ik_y y)]\exp(ik_x x - i\omega t), \tag{55}$$

and the corresponding magnetic field can be given by

$$\mathbf{H} = \frac{1}{i\omega}\left(\frac{\mathbf{e_x}}{\mu_{xx}^e}\frac{\partial E_z}{\partial y} - \frac{\mathbf{e_y}}{\mu_{yy}^e}\frac{\partial E_z}{\partial x}\right). \tag{56}$$

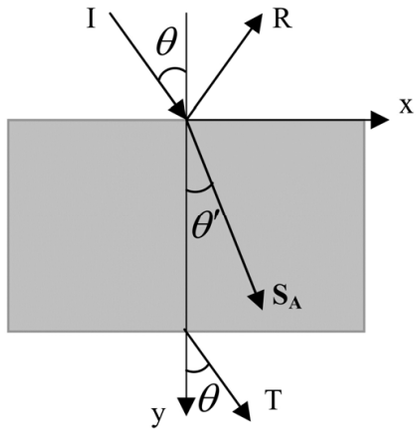

Figure 11. Draft for incidence, reflection, refraction and transmission rays. After Wang & Song, 2009.

The radiation in the film consists of two parts, one is the forward light (refraction light) related to amplitude A_0 and the other is the backward light (reflection light) related to amplitude B_0 . Here, k_y is defined as a negative number, otherwise the refraction wave corresponds to amplitude B_0 . These two situations are equivalent in essence. According to the definition of energy flow density of electromagnetic wave $\mathbf{S} = \mathrm{Re}(\mathbf{E} \times \mathbf{H}^*)/2$, the flow densities of the two lights can be given by

$$\mathbf{S_A} = \mathrm{Re}\left[\frac{|A_0|^2}{2\omega}\left(\frac{k_x}{\mu_{yy}^e}\mathbf{e_x} + \frac{k_y}{\mu_{xx}^e}\mathbf{e_y}\right)\right], \mathbf{S_B} = \mathrm{Re}\left[\frac{|B_0|^2}{2\omega}\left(\frac{k_x}{\mu_{yy}^e}\mathbf{e_x} - \frac{k_y}{\mu_{xx}^e}\mathbf{e_y}\right)\right]. \tag{57}$$

The inner product between a wave vector ($\mathbf{K_A} = [k_x, k_y, 0]$ or $\mathbf{K_B} = [k_x, -k_y, 0]$) and its corresponding energy flow is given by expression $I_A = \mathrm{Re}(\varepsilon_{zz}^e \omega |A_0|^2)/2$, or $I_B = \mathrm{Re}(\varepsilon_{zz}^e \omega |B_0|^2)/2$. Thus the angle between energy flow and wave vector can be expressed as

$$\alpha_j = \arccos[I_j / (|\mathbf{K_j}||\mathbf{S_j}|)], \tag{58}$$

where *j*=*A* or *B*. It is obvious that α_A is equal to α_B and larger than $\pi/2$ in the range (52).

It can be seen from the expression (57) of $\mathbf{S_A}$ that its x component is negative and y component is positive when both $\mu_{xx}^e < 0$ and $\mu_{yy}^e < 0$, since k_x is positive and identical to the equivalent component of the incident wave vector. Thus an important condition is found for the existence of negative refraction, or AF layers must be thicker than IC layers. The refraction angle can be expressed as

$$\theta' = \arctan(k_x \mu_{xx}^e / k_y \mu_{yy}^e). \tag{59}$$

FeF_2 and TlBr are used as constituent materials where the AF resonant frequency ω_r is closer to the phonon resonant frequency ω_T and located in the far infrared regime. Fig.12 shows this angle as a function of frequency for $f_a = 0.8$ and 0.6. It can be seen from Fig.12 that for most of the frequency range occupied by the curves, angle α is at least bigger than 160^o for various incident angles. So the wave vector, electric and magnetic fields form an approximate left-handed triplet. The operation frequency range becomes narrow as f_a decreases, as shown in Fig.12b.

As shown in Fig.13(a) for $f_a = 0.8$, the refraction angle is positive on the left side and negative on the right side of the intersection point of the curves. This corresponds to the following critical frequency obtained under the condition of $\mu_{xx}^e < 0$ and $\mu_{yy}^e < 0$:

$$\omega_c = \sqrt{\omega_r^2 + 2 f_i \omega_m \omega_a}. \tag{60}$$

It can be seen from Fig.13(b) in comparing with Fig.13(a) that the frequency region of negative refraction is obviously narrower and the negative refraction angle becomes smaller. Numerical simulations also show both positive and negative refraction angles are in the spectral range of approximate left-handed feature shown in Fig.12.

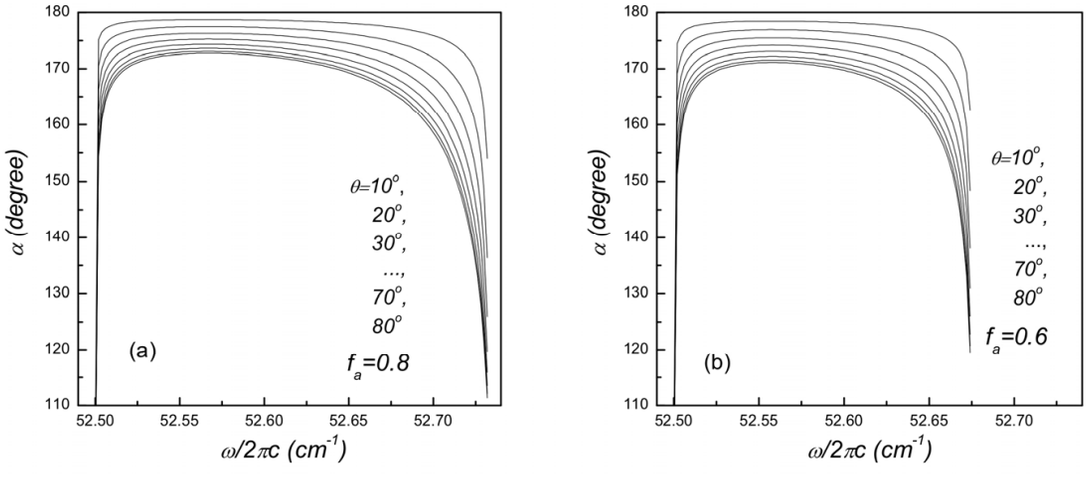

Figure 12. Angle α beteen refraction energy flow and corresponding wave vector versus frequency for different incident angles and for filling ratios (a) $f_a = 0.8$ and (b) $f_a = 0.6$. After Wang & Song, 2009.

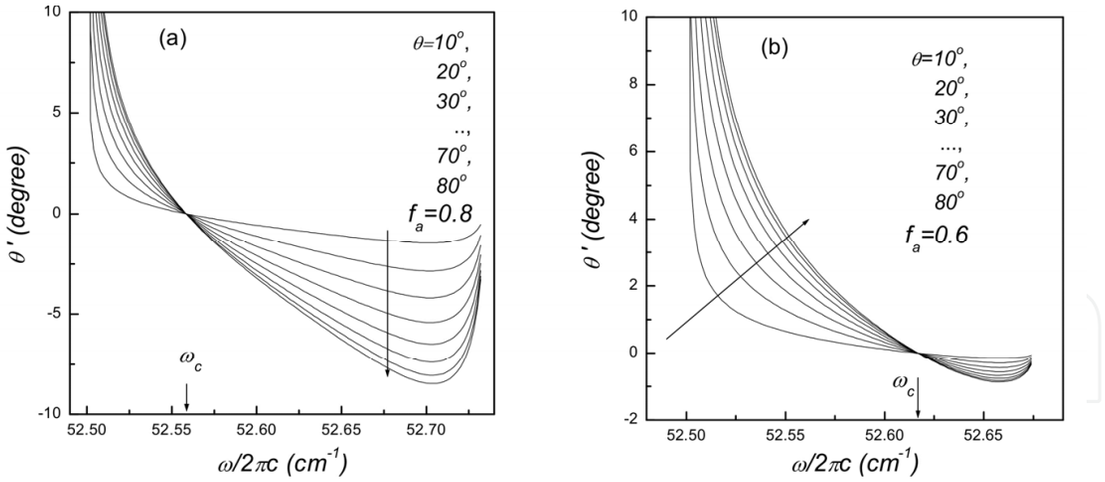

Figure 13. Refraction angle versus frequency for various incident angles, and for filling ratios (a) $f_a = 0.8$ and (b) $f_a = 0.6$. After Wang & Song, 2009.

4. Transmission, refraction and absorption properties of AF/IC PCs

In this section, we shall examine transmission, refraction and absorption of AF/IC PCs, where the condition of the period much smaller than the wavelength is not necessary. The transmission spectra based on FeF2/TIBr PCs reveal that there exist two intriguing guided modes in a wide stop band [11]. Additionally, FeF2/TIBr PCs possess either the negative refraction or the quasi left-handedness, or even simultaneously hold them at certain frequencies of two guided modes, which require both negative magnetic permeability of AF layers and negative permittivity of IC layers. The handedness and refraction properties of the system can be manipulated by modifying the external magnetic field which will determine the frequency regimes of the guided modes.

The geometry is shown in Fig. 1. We assume the electric field solutions in AF and IC layers as

$$\vec{E}_j = \vec{e}_z[A_j \exp(ik_j y) + B_j \exp(-ik_j y)]\exp(ik_x x - i\omega t), \tag{61}$$

where $j = a, i$ signify AF or IC layers, respectively. The corresponding magnetic field solutions are also achieved via $\nabla \times \vec{E}_j = i\omega \vec{B}_j$. According to the boundary conditions of E_z and H_x continuous at interfaces, the relation between wave amplitudes in the two same layers of the two adjacent periods can be shown as a transfer matrix $\ddot{\mathrm{T}}$ [43]. The matrix elements are expressed by the following equations:

$$T_{11} = \delta_a[(\Delta - \Delta')\cos(k_i d_i) + i(1 - \Delta\Delta')\sin(k_i d_i)]/(\Delta - \Delta'), \tag{62}$$

$$T_{12} = i\delta_a^{-1}(1 - \Delta'^2)\sin(k_i d_i)/(\Delta - \Delta'), \tag{63}$$

$$T_{21} = i\delta_a(\Delta^2 - 1)\sin(k_i d_i)/(\Delta - \Delta'), \tag{64}$$

$$T_{22} = \delta_a^{-1}[(\Delta - \Delta')\cos(k_i d_i) + i(\Delta\Delta' - 1)\sin(k_i d_i)]/(\Delta - \Delta') \tag{65}$$

with $\Delta = \left(ik_x\mu_\perp/\mu + k_a\right)/k_i\mu_\nu$ and $\Delta' = \left(ik_x\mu_\perp/\mu - k_a\right)/k_i\mu_\nu$. In AF layers, there are the relation $k_a^2 = \varepsilon_a\mu_v\omega^2/c^2 - k_x^2$ with $\mu_v = \left(\mu^2 - \mu_\perp^2\right)/\mu$, $k_x^2 = \omega^2/c^2\sin^2\theta$ and ε_a the dielectric constant. The magnetic permeability tensor components of AF layers are represented by

$$\mu = 1 + \omega_m\omega_a\{1/[\omega_r^2 - (\omega_0 - \omega - i\sigma)^2] + 1/[\omega_r^2 - (\omega_0 + \omega + i\sigma)^2]\}, \tag{66}$$

$$\mu_\perp = \omega_m\omega_a\{1/[\omega_r^2 - (\omega_0 - \omega - i\sigma)^2] - 1/[\omega_r^2 - (\omega_0 + \omega + i\sigma)^2]\}. \tag{67}$$

with $\omega_m = 4\pi\gamma M_0$, $\omega_a = \gamma H_a$, $\omega_r = [\omega_a(2\omega_e + \omega_a)]^{1/2}$, $\omega_e = \gamma H_e$ and $\omega_0 = \gamma H_0$. M_0 represents the sublattice magnetization, and H_0, H_a and H_e indicate the external magnetic field, anisotropy and the exchange fields, respectively. ω_r denotes the zero-field resonant frequency, γ and σ are the gyromagnetic ratio and the magnetic damping. In IC layers, we have the relation $k_i^2 = \varepsilon_i\omega^2/c^2 - k_x^2$ with the dielectric function $\varepsilon_i = \varepsilon_h + \left\{(\varepsilon_l - \varepsilon_h)\omega_T^2\right\}/\left(\omega_T^2 - \omega^2 - i\xi\omega\right)$, where ε_h and ε_l are the high- and low-frequency dielectric constants, but ω_T indicates the frequency of the TO vibrating mode in the long-wavelength limition and ξ denotes the phonon damping. The magnetic permeability of IC layers is considered as $\mu_i = 1$. We assume here that the stacking number included in the magnetic superlattices is *N*. Then transmission and reflection coefficients of the AISL can be written as

$$\begin{pmatrix}1\\ r\end{pmatrix} = \frac{1}{2}\begin{pmatrix}1+\Delta_1 & 1+\Delta_1'\\ 1-\Delta_1 & 1-\Delta_1'\end{pmatrix}\vec{T}^{N-1}\begin{pmatrix}k_i\delta_a\delta_i(1+\Delta)/(k_1+k_i) & k_i\delta_a^{-1}\delta_i(1+\Delta')/(k_1+k_i)\\ k_i\delta_a\delta_i^{-1}(1-\Delta)/(k_i-k_1) & k_i\delta_a^{-1}\delta_i^{-1}(1-\Delta')/(k_i-k_1)\end{pmatrix}\begin{pmatrix}t\\ t\end{pmatrix}. \tag{68}$$

Note that incident wave amplitude is taken as 1. Therefore, the transmission and reflection coefficients can be determined with Eq. (68), and then the transmission ratio is $|t|^2$ and reflection ratio is $|r|^2$. Additionally, absorption ratio is represented with $A = 1 - |r|^2 - |t|^2$. Other quantities in Eq. (68) are $\Delta_1 = \left(ik_x\mu_\perp/\mu + k_a\right)/k_1\mu_\nu$, $\Delta_1' = \left(ik_x\mu_\perp/\mu - k_a\right)/k_1\mu_\nu$, $\delta_i = \exp(ik_i d_i)$, $k_1^2 = \omega^2/c^2\cos^2\theta$.

As described in Ref. [8], magnetic superlattices possess two mini-bands with negative group velocity. When the incident wave is located in the frequency regions corresponding to the two mini-bands, what are the optical properties of the AF/IC PCs? In the preceding section, the expressions of transmission and absorption to be used have been derived. To grasp handedness and refraction properties of the AF/IC PCs, the refraction angle and propagation direction need to be determined. Therefore, subsequently we give the expression of the refraction angle. However, this structure possibly possesses a negative refraction, and generally the directions of the energy flow of electromagnetic wave and the wave vector misalign. We start with the definition of energy flow ($\vec{S} = \mathrm{Re}[\vec{E}\times\vec{H}^*]/2$) with a

view to achieving refraction properties. Based on wave solutions of the electric field and Maxwell equations, the magnetic field components of the forward-going wave in AF layers are shown as

$$H_{ax} = \frac{(k_a + ik_x\mu_\perp / \mu)}{\omega\mu_0\mu_\nu} A_a \exp(ik_a y + ik_x x - i\omega t). \tag{69}$$

$$H_{ay} = \frac{(ik_a\mu_\perp / \mu - k_x)}{\omega\mu_0\mu_\nu} A_a \exp(ik_a y + ik_x x - i\omega t). \tag{70}$$

The magnetic field components of the forward-going wave in the adjacent IC layers are

$$H_{ix} = \frac{k_i A_i}{\omega\mu_0}\exp(ik_i y + ik_x x - i\omega t),\ H_{iy} = -\frac{k_x A_i}{\omega\mu_0}\exp(ik_i y + ik_x x - i\omega t). \tag{71}$$

The amplitudes of two neighboring layers satisfy

$$\begin{pmatrix} A_i \\ B_i \end{pmatrix} = \begin{pmatrix} (1+\Delta_1)\delta_a & (1-\Delta_2)\delta_a^{-1} \\ (1-\Delta_1)\delta_a & (1+\Delta_2)\delta_a^{-1} \end{pmatrix} \begin{pmatrix} A_a \\ B_a \end{pmatrix} \tag{72}$$

According to boundary conditions, the electric and magnetic fields of every layer are acquired when the incident wave is known. Then the expressions of refraction energy flow in all layers are written as

$$\vec{S}_j = \mathrm{Re}\left(\vec{E}_j \times \vec{H}_j^{\,*}\right)\Big/2 = \mathrm{Re}\left(-H_{jy}^* E_{jz}\vec{e}_x + E_{jz}H_{jx}^*\vec{e}_y\right)\Big/2,\ \left(j = a, i\right). \tag{73}$$

What needs to be emphasized is that we here concentrate only on the refraction, so only the forward-going wave corresponding to the first term in Eq.(61) is considered and the backward-going wave is ignored. Owing to refraction angles being different in various layers, the refraction angle of the AF/IC PCs should be effective one. The angle between the energy flow and wave vector, and the refraction angle of the AF/IC PCs are defined as

$$\alpha = \arccos[(\vec{K}\cdot\vec{S}) / (\left|\vec{K}\right|\left|\vec{S}\right|)], \tag{74}$$

$$\theta' = arctg[(f_1 S_{ax} + f_2 S_{ix}) / (f_1 S_{ay} + f_2 S_{iy})], \tag{75}$$

with $\vec{K} = k_x\vec{e}_x + \left(f_1 k_a + f_2 k_i\right)\vec{e}_y$ and $\vec{S} = f_1\vec{S}_a + f_2\vec{S}_i$, where volume fractions are $f_1 = d_a\big/\left(d_a + d_i\right)$ and $f_2 = 1 - f_1$, respectively.

Numerical calculations based on FeF_2/TlBr PCs. We take the AF layer thickness $d_a = 4\mu m$ and the thickness of IC layers $d_i = 1\mu m$. The stacking number is $N = 9$. Figure 14 shows the transmission spectra with specific angles of the incidence in an external magnetic field $H_0 = 3T$. As illustrated in Fig. 14(a), the forbidden band ranges from $0.9\omega_r$ to $1.2\omega_r$

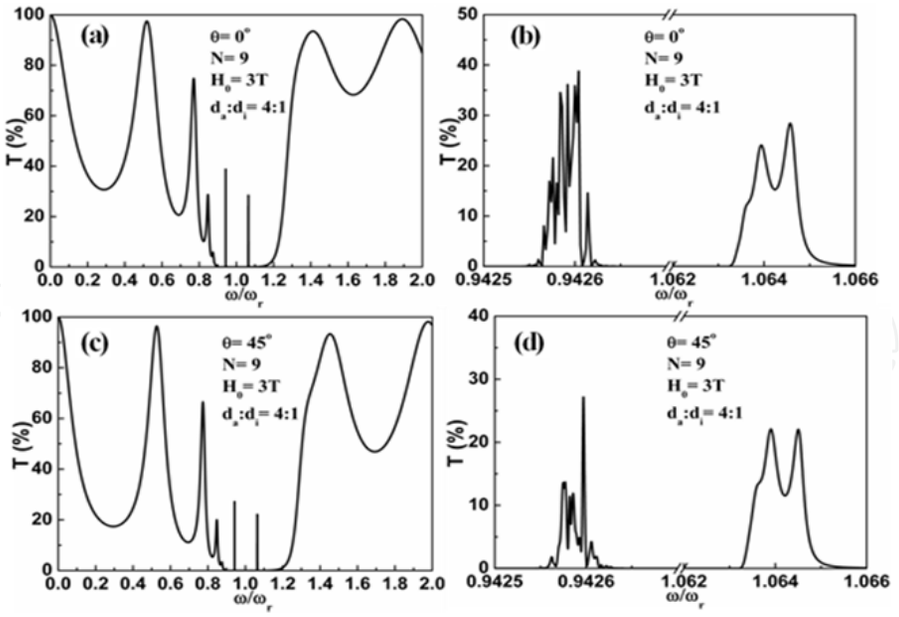

Figure 14. Transmission spectra for the fraction $f_1 = 0.8$, external magnetic field $H_0 = 3\,T$ and stacking number $N = 9$. (a) the incident angle $\theta = 0^0$; (b) a zoomed view of guided modes in (a); (c) the incident angle $\theta = 45^0$; (d) a zoomed view of guided modes in (c). After Wang & Ta, 2012.

corresponding to the band gap of magneto-phonon polariton in Ref. [8]. Here the most interesting may be that guided modes arise in the forbidden band. The two guided modes lie in the proximity of $\omega = 0.943\omega_r$ and $\omega = 1.064\omega_r$, corresponding to the mini-bands with negative group velocity in Ref. [8]. At the same time, the magnetic permeability of AF layers and the dielectric function for IC layers are both negative. To distinctly observe two guided modes, the partially enlarged Fig. 14(b) corresponding to Fig. 14(a) is exhibited. Seen from Fig. 14(b), the maximum transmission of the guided mode with lower-frequency is 40% and that of higher mode is 28.4%. As is well known, the optical thicknesses of films are determined by the frequency-dependent magnetic permeability and the dielectric function. Then the optical thicknesses of thin films are varied with the frequency of incident wave. The optical path of wave in media can also be altered by changing the incident angle. Fig. 14(c) shows the transmission spectrum with incident angle 45^o and other parameters are the same as those in 14(a). The partially enlarged Fig. 14(d) corresponding to Fig. 14(c) is given. Compared with the normal incidence case, for $\theta \neq 0$ the forbidden band becomes wide and their maximum transmissions are reduced to 27.1% and 21.9%, but two guided modes keep their frequency positions unaltered.

As already noted, the damping is included and then the absorption appears. We are more interest in the two guided modes, so only the absorption corresponding to two guided modes will be considered in Fig. 15 (a) and (c) display the absorption spectra in the case of right incidence, but (b) and (d) illustrate the absorption spectra for incident angle $\theta = 45^o$. We see that the absorption has a great influence on the transmission spectra. In the absorbing band at $\omega = 0.9426\omega_r$, relative tiny absorption corresponds exactly to the

maximum transmission. In the absorbing band at $\omega = 1.024\omega_r$, the absorption is obviously strengthened with enhancing the incident angle.

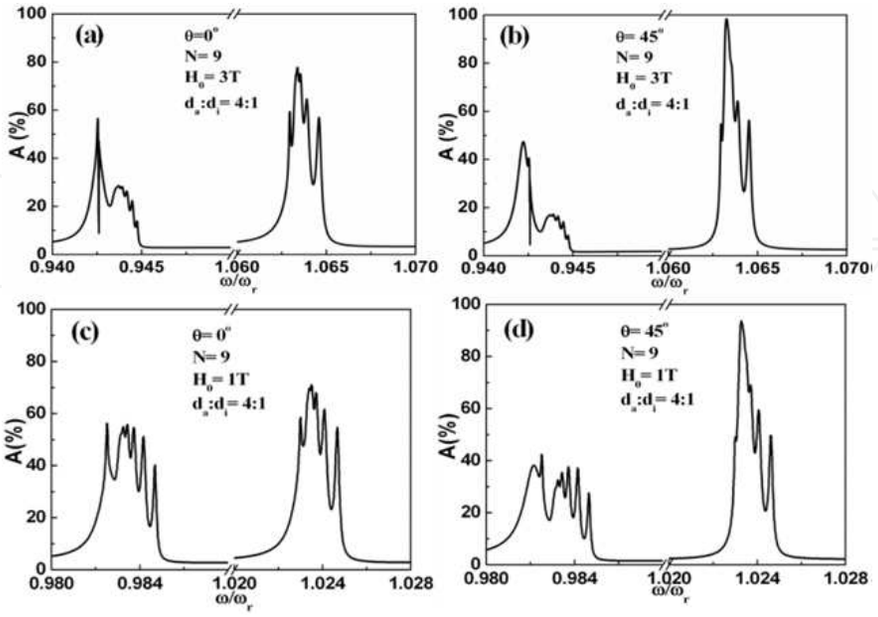

Figure 15. Partially enlarged absorption spectra with $f_1 = 0.8$, $N = 9$, $H_0 = 3\,T$ and $H_0 = 1\,T$. (a) corresponding to Fig. 14(b); (b) corresponding to Fig.14(d); (c) corresponding to Fig. 15(b); (d) corresponding to Fig. 15(d). After Wang & Ta, 2012.

To capture the handedness and refraction behaviors of the AF/IC PCs, the angle of refraction and the angle between the energy flow and wave vector are illustrated. Fig. 16 shows the angle α between the energy flow and wave vector of forward-going wave varies with frequency for $H_0 = 3\,T$ and $\theta = 45^{\circ}$. As illustrated in Fig. 16, the angles in the vicinities of $\omega = 0.943\omega_r$ and $\omega = 1.064\omega_r$ are greater than 90°, but less than 180°. It indicates that the AF/IC PCs possesses a quasi left-handedness in these frequency regions.

Figure 17 shows the refraction angle θ' versus frequency under the same condition as Fig. 16. We find the refraction angles are negative in the neighborhood of $\omega = 0.943\omega_r$ and $\omega = 1.064\omega_r$. The two frequency ranges for negative angle do not completely coincide with those of the quasi-left-handedness in Fig. 17. Namely, the frequency regime of negative refraction near to $\omega = 0.943\omega_r$ is strikingly greater than that occupied by the quasi-left-handedness in Fig.17. However, the result is opposite in the vicinity of $\omega = 1.064\omega_r$. Therefore, we here reckon the left-handedness is not always accompanied by negative refraction. FeF_2/TlBrsuperlattices have the natures of either negative refraction or quasi left-handedness, or even simultaneously bear them at the certain frequencies of two guided modes.

To have a deeper understanding of the negative refraction and quasi- left-handedness of the AF/IC PCs, subsequently the expressions of the dielectric function

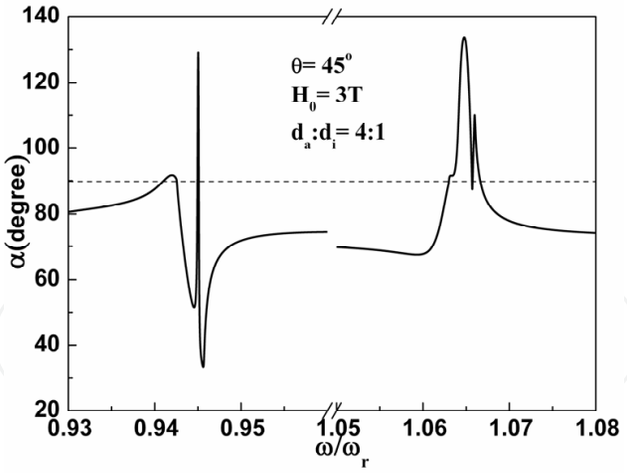

Figure 16. Angle α between energy flow and wave vector of down going wave versus the change of frequencies at $H_0 = 3\,T$, $\theta = 45^0$ and $f_1 = 0.8$. After Wang & Ta, 2012.

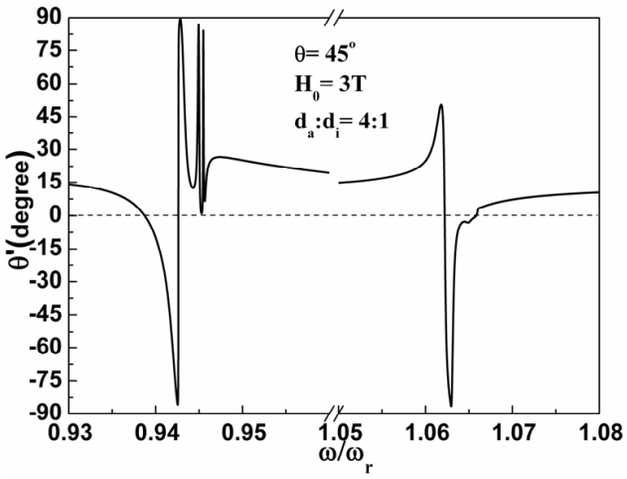

Figure 17. Refraction angle θ' versus the alteration of frequencies at $H_0 = 3\,T$, $\theta = 45^0$ and $f_1 = 0.8$. After Wang & Ta, 2012.

$\varepsilon_i = \varepsilon_h + \left\{(\varepsilon_l - \varepsilon_h)\omega_T^2\right\} \Big/ \left(\omega_T^2 - \omega^2 - i\xi\omega\right)$ of IC layers and the magnetic permeability of AF layers are analyzed. We find that when frequency lies in

$$\omega_T < \omega < \left(\varepsilon_l / \varepsilon_h\right)^{1/2} \omega_T, \tag{76}$$

the dielectric function ε_i is negative, namely the range $0.9152\omega_r < \omega < 2.1835\omega_r$. This completely covers the frequency range of AF resonance, so the dielectric function must be negative in the region of negative magnetic permeability μ_v. It is found from Fig.18 that the magnetic permeability μ_v is negative in certain regions, where the dielectric function ε_i is also negative. In our previous work [8], utilizing the effective medium theory, we verified the effective dielectric function and magnetic permeability are both negative in the long wavelength limit when μ_v and ε_i are negative. In other words, the AF/IC PCs is of negative

refraction in the limit of long wavelength. Regarding the results arising from the two methods mentioned above, we conclude that the necessary condition of negative refraction or left-handedness is that μ_v and ε_i are both negative in this PCs.

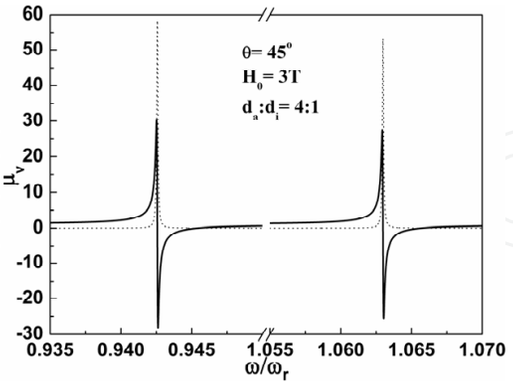

Figure 18. Voigt magnetic permeability μ_v versus the different frequencies at $H_0 = 3\,T$, $\theta = 45^0$ and $f_1 = 0.8$ (solid line denotes real parts and broken line indicates imaginary parts). After Wang & Ta, 2012.

5. Summary

This chapter aims to discover optical properties of AF/IC PCs in the presence of external static magnetic field. First, within the effective-medium theory, we investigated dispersion properties of MPPs in one- and two-dimension AF/IC PCs. The ATR (attenuated total reflection) technique should be powerful in probing these MPPs. Second, there is a frequency region where the negative refraction and the quasi left-handedness appear when the AF/IC PCs period is much shorter than the incident wavelength. Finally, an external magnetic field can be used to modulate the optical properties of the AF/IC PCs.

Author details

Shu-Fang Fu and Xuan-Zhang Wang
Key Laboratory for Photonic and Electronic Bandgap Materials, Ministry of Education, School of Physics and Electronic Engineering, Harbin Normal University, Harbin, China

Acknowledgement

This work was financially supported by the National Natural Science Foundation of China with Grant no.11084061, 11104050, and the Natural Science Foundation of Heilongjiang Province, with no. ZD200913.

6. References

[1] T. Goto, A .V. Baryshev, M. Inoue, A. V. Dorofeenko, A. M. Merzlikin, A. P. Vinogradov, A. A. Lisyansky, A. B. Granovsky, Tailoring surfaces of one-dimensional

magnetophotonic crystals: optical Tamm state and Faraday rotation, Phys. Rev. B. 79 (2009) 125103/1-5.
[2] R. H. Zhu, S. N. Fu, H. Y. Peng, Far infrared Faraday rotation effect in one-dimensional microcavity type magnetic photonic crystals, J. Magn. Magn. Mater. 323 (2011) 145-149.
[3] X. Z. Wang, The Faraday effect of an antiferromagnetic photonic crystal with a defect layer, J. Phys.:Condens. Matter. 17 (2005) 5447-5452.
[4] V. V. Pavlov, P. A. Usachev, R. V. Pisarev, D. A. Kurdyukov, S. F. Kaplan, A. V. Kimel, A. Kirilyuk, Th. Rasing, "Enhancement of optical and magneto-optical effects in three-dimensional opal/Fe3O4 magnetic photonic crystals," Appl. Phys. Lett. 93 (2008) 072502/1-3.
[5] V. V. Pavlov, P. A. Usachev, R. V. Pisarev, D. A. Kurdyukov, S. F. Kaplan, A. V. Kimel, A. Kirilyuk, Th. Rasing, "Optical study of three-dimensional magnetic photonic crystals opal/Fe3O4," J. Magn. Magn. Mater. 321 (2009) 840-842.
[6] R. Atkinson, "Limits of enhancement of the Faraday effect in ultra-thin magnetic layers by one-dimensional magnetophotonic crystals, "J. Phys. D: Appl. Phys. 39 (2006) 999-1005.
[7] M.M. Sigalas, C.M. Soukoulis, R. Biswas, K.M. Ho, "Effect of the magnetic permeability on photonic band gaps," Phys. Rev. B 56, (1997) 959-962.
[8] J. X. Ta, Y. L. Song, X. Z. Wang, "Magneto-phonon polaritons of antiferromagnetic/ion-crystal superlattices," J. Appl. Phys. 108 (2010) 013520/1-4.
[9] J. X. Ta, Y. L. Song, X. Z. Wang, "Magneto-phonon polaritons in two-dimension antiferromagnetic/ion-crystalic photonic crystals," Photonics and Nanostructures - Fundamentals and Applications 10(2012)/ 1-8.
[10] Y. L. Song, J. X. Ta, H. Li, X. Z. Wang, "Presence of left-handedness and negative refraction in antiferromagnetic/ionic-crystal multilayered films, " J. Appl. Phys. 106 (2009) 063119/1-4.
[11] J. X. Ta, Y. L. Song, X. Z. Wang, "Optical properties of antiferromagnetic/ion-crystal superlattices," J. Magn. Magn. Mater. 324 (2012) 72-74.
[12] J. B. Pendry, "Negative refraction makes a perfect lens," Phys. Rev. Lett. 85, (2000) 3966-3969.
[13] D. R. Smith and N. Kroll, "Negative refractive index in left-handed materials," Phys. Rev. Lett. 85, (2000) 2933-2936.
[14] D. Schurig and D. R. Smith, "Negative index lens aberrations," Phys. Rev. E 70, (2004) 065601-1-4.
[15] R. A. Shelby, D. R. Smith, and S. Schultz, "Experimental verification of a negative index of refraction," Science 292, (2001)77-79.
[16] D. R. Smith, W. J. Padilla, D. C. Vier, S. C. Nemat-Nasser, and S. Schultz, "Composite medium with simultaneously negative permeability and permittivity," Phys. Rev. Lett. 84, (2000) 4184-4187.
[17] W. T. Lu, J. B. Sokoloff, and S. Sridhar, "Refraction of electromagnetic energy for wave packets incident on a negative-index medium is always negative," Phys. Rev. E 69, (2004) 026604-1-5.

[18] C. G. Parazzoli, R. B. Greegor, K. Li, B. E. C. Koltenbah, and M. Tanielian, "Experimental verification and simulation of negative index of refraction using Snell's law," Phys. Rev. Lett. 90, (2003)107401-1-4.
[19] A. A. Houck, J. B. Brock, and I. L. Chuang, "Experimental observations of a left-handed material that obeys Snell's law," Phys. Rev. Lett. 90, (2003)137401-1-4.
[20] Zhaolin Lu, Janusz A. Murakowski, Christopher A. Schuetz, Shouyuan Shi, Garrett J. Schneider, and Dennis W. Prather, "Three-dimensional subwavelength imaging by a photonic-crystal flat lens using negative refraction at microwave frequencies," Phys. Rev. Lett. 95, (2005)153901-1-4.
[21] J. Lezec Henri, A. Dionne Jennifer, and A. Atwater Harry, "Negative refraction at visible frequencies," Science 316, (2007)430-432.
[22] A. Berrier, M. Mulot, M. Swillo, M. Qiu, L. Thylen, A. Talneau, and S. Anand, "Negative refraction at infrared wavelengths in a two-dimensional photonic crystal," Phys. Rev. Lett. 93, (2004) 073902-1-4.
[23] W. T. Lu and S. Sridhar, "Superlens imaging theory for anisotropic nanostructured metamaterials with broadband all-angle negative refraction," Phys. Rev. B 77, (2008) 233101-1-4.
[24] F. M. Wang, H. Liu, T. Li, Z. G. Dong, S. N. Zhu, and X. Zhang, "Metamaterial of rod pairs standing on gold plate and its negative refraction property in the far-infrared frequency regime," Phys. Rev. E 75, (2007) 016604-1-4.
[25] Andrea Alu and Nader Engheta, "Three-dimensional nanotransmission lines at optical frequencies: A recipe for broadband negative-refraction optical metamaterials," Phys. Rev. B 75, (2007) 024304-1-20.
[26] R.H. Tarkhanyana and D.G. Niarchos, "Wave refraction and backward magnon–Plasmon, polaritons in left-handed antiferromagnet/semiconductor superlattices," J. Magn. Magn. Materials, 312, (2007) 6-15.
[27] C. F. Klingshirn, Semiconductor Optics (Springer, Berlin 1997) Ch.13.
[28] A.D. Boardman, Electromagnetic Surface Modes, John Wiley, New York, 1982.
[29] R. T. Tagiyeva, M. Saglam,"Magnetic polaritons at the junctions of magnetic superlattice and magnetic material." Solid State Commun. 122 (2002) 413-417.
[30] N.Raj, D.R.Tilley, "Polariton and effective-medium theory of magnetic Superlattices ," Phys.Rev. B 36, (1987) 7003-07.
[31] Na Liu, Xiao-Dong Hou, Xiangdong Zhang, J. "Retarded modes in layered magnetic structures containing left-handed materials," Phys. Condens. Matter 20, (2008) 335210/1-5.
[32] C.A.A.Araújo, E.L.Albuquerque, D.H.A.L.Anselmo, M.S. Vasconcelos,"Magnetic polaritons in metamagnet layered structures: Spectra and localization properties," Phys. Lett. A 372, (2008) 1135-1140.
[33] Xuan-Zhang Wang, Tilley. D. R, "Retarded modes of a lateral antiferromagnetic /nonmagnetic superlattice," Phys. Rev. B 52, (1995) 13353-13357.
[34] M. C. Oliveros, N. S. Almeida, D. R. Tilley, J. Thomas, R. E. Camley, "Magnetostatic modes and polaritons in antiferromagnetic-non-magnetic superlattices," J. Phys. Condens. Matter 4, (1992) 8497-8510.

[35] I. Balin, N. Dahan, V. Kleiner, E. Hasman, "Slow surface phonon polaritons for sensing in the midinfrared spectrum," Appl. Phys. Lett. 94 , (2009) 111112/1-3.
[36] A. J. Huber, B. Deutsch, L. Novotny, R. Hillenbrand, "Focusing of surface phonon polaritons," Appl. Phys. Lett. 92 , (2008) 203104/1-3.
[37] K. Abraha, D.E. Brown, T. Dumelow, T.J. Parker, D.R. Tilley, "Obliqu-incidence far-infrared reflectivity study of the uniaxial antiferromagnet FeF2," Phys. Rev. B 50 ,(1994) 6808-6816.
[38] E.D. Palik, Handbook of Optical Constants, Vol.3, Academic Press, San Diego, 1998, pp.926; R.C. Fang, Solid State Spectroscopy, Press., Univ. of Sci. and Tech. of China, Hefei, 2001, pp. 234 (in Chinese).
[39] Xuan-Zhang Wang and Hua Li, Nonlinear propagation of electromagnetic waves in antiferromagnets, in Propagation of Electromagnetic Waves in Complex Matter, edited by Ahmed Kishk, (Intech-Open Access Publisher, 2011)pp.55-96, Ch.3
[40] X.Z. Wang, D.R. Tilley, "Magnetostatic surface and guided modes of lateral-magnetic-superlattice films," Phys. Rev. B 50, (1994) 13472-13479.
[41] X.Z. Wang, X.R. Xu, "Nonlinear Magnetostatic surface waves of magnetic multilayers: Effective-medium theory," Phys. Rev. B 63, (2001) 054415/1-11.
[42] D.N. Mirlin, in: V.M. Agranovich, D.L. Mills (Eds.), Surface phonon polaritons in dielectrics and semiconductors, in Surface Polaritons, North-Holland Press, Amsterdam, 1982, pp. 5-67.
[43] X. F. Zhou, J. J. Wang, X .Z. Wang, D.R. Tilley, "Reflection and transmission by magnetic multilayers," J. Magn. Magn. Mater. 212, (2000) 82-90.